# Steps Toward Efficient Processing of Handwritten Signature Images

**Robert Sabourin*** **and Réjean Plamondon****

* Laboratoire Scribens, Ecole de Technologie Supérieure, Département de Génie de la Production Automatisée, 4750 Henri-Julien, Montréal QC, H2T 2C8

** Laboratoire Scribens, Ecole Polytechnique de Montréal, Département de Génie Electrique, C.P. 6079, Succ. "A", Montréal QC, H3C 3A7

## Abstract

Basic research work in the field of Automatic Handwritten Signature Verification Systems (AHSVS) has been carried out for more than ten years at the Scribens Laboratory. This paper reports on the latest achievements in the AHSVS using gray-level images that we proposed recently [4-6]. A novel handwritten signature representation permits the local analysis of gray levels along the signature line, permitting the elimination of various classes of forgeries, i.e. random, tracing, photocopy, simulated and freehand. This work demonstrates the fact that skilled forgeries that show a great dissimilarity in contrast between primitives pairs located on solution path N can be discriminated successfully.

## Résumé

De nombreux travaux de recherche ont été réalisés au Laboratoire Scribens depuis les dix dernières années, notamment dans le domaine de la vérification automatique de l'identité. Cet article présente les derniers résultats expérimentaux obtenus avec l'utilisation des images de signatures manuscrites [4-6]. Une nouvelle représentation des images de signatures manuscrites permet l'analyse locale de la luminance dans le trait de la signature. Cette nouvelle approche favorise l'élimination de diverses classes de faux; les faux aléatoires, les calques, les photocopies, les faux avec imitation servile et les faux avec imitation libre. Les résultats expérimentaux présentés dans cet article permettent d'avancer le fait que les faux caractérisés par une forme similaire à la signature authentique peuvent être éliminés si une différence de contraste suffisamment élevée subsiste entre les paires de primitives localisées sur le chemin solution N.

**Keywords:** Automatic Signature Verification, Structural Pattern Recognition, Scene Understanding, Computer Vision

## 1. Introduction

A recent survey of the litterature on automatic signature verification and writer identification by computer has been presented by Plamondon and Lorette [1]; all systems proposed in the field of AHSVS using gray-level images show an upper limit to the total minimum error rate of $\varepsilon_{tmin} \approx 5\%$. The best experimental results have been obtained by Ammar et al. [7] with a type I error rate of $\varepsilon_1 = 6\%$ and a type II error rate of $\varepsilon_2 = 4\%$ (simulated forgeries), Nouboud et al. [12,13] with $\varepsilon_1 = 2\%$ and $\varepsilon_2 = 8\%$ (random forgeries), and finally by Brocklehurst [14] with $\varepsilon_1 = 5\%$ and $\varepsilon_2 = 5\%$ (simple forgeries). Moreover, all AHSVS failed with tracings and photocopies, producing 100% of Type II error rates.

A feasibility study [2] has shown that features derived from the direc-

tional space can discriminate efficiently between classes of writers. The use of graphometric features (that is to say, characteristics used by the expert document analysts [15]) taken interactively reveals that structural measurements are powerful enough for the elimination of simulated forgeries [3]. From these exploratory experiments, a model-based system dedicated to the interpretation of handwritten signature images has been built around a novel signature representation [4-6], permitting the local analysis of gray levels along the signature line; this approach allows the elimination of tracings and photocopies showing a great local dissimilarity in gray levels.

## 2. Data acquisition and Preprocessing

The data acquisition process takes into account the video signal f(i,j) coming from a vidicon camera and is sampled with a spatial resolution of 128x512 pixels. The resulting gray-level image is then analysed by the preprocessing phase which is subdivided into two stages, the gradient computation and the background elimination processes. The gradient at locations (m,n) is evaluated over the entire gray-level image with the Sobel operator. The resulting filtered image is then analysed by the background elimination process. Because the handwritten signature line is characterized by a high gradient activity, the density function $F(|\nabla|)$ is computed and a threshold T is automatically settled [2]. Finally, all pixels at location (m,n) with a high gradient activity, that is to say $|\nabla|(m,n) \geq T$, are labelled as signal pixels. Pixels not satisfying the latter constraint are labelled as background pixels.

## 3. Primitive Extraction (PE)

The signature image is afterwards analysed by the primitive extraction process [4,5], which is responsible for the production of the primitive sets necessary for the structural interpretation of the handwritten signature by the comparison process [6]. The strategy adopted in the primitive extraction process takes into account the collinearity of neighbouring signal pixels in the directional plane of the gradient space. This task is also performed in two stages. First, a Region-Growing-With-Merging process (RGWM) [4] growth the signal pixels into atomic regions characterized by the uniformity of a local property, i.e. the orientation of their gradient vectors. The resulting atomic regions belong to the signature line or represent spurious noise elsewhere in the scene.

The word, "ah!", depicted in Figures 1a and 1b, will serve as a case study to illustrate the various stages of the AHSVS. The goal of this experiment is to evaluate a static similarity measure $\vartheta_S(Pr,Pt)$ between the reference image (Figure 1a) and the test image (Figure 1b). As stated previously, the RGWM process applied to the gray-level image in Figure 1a produces the atomic region set shown in Figure 1c. The cardinality of the resulting atomic region set is Nr = 408 regions. An enlargement of the letter "a" depicted in Figure 1d shows the atomic region partitions in the gradient space.

The second stage of the primitive extraction process is responsible for generating the primitive set that is related to the signature line. As shown in Figure 1e, the High-Level-Merging process (HLM) begins with the elimination of sparse atomic regions, resulting in Nr = 82 regions. The HLM process continues with a hierarchical merging scheme, and takes advantage of neighbouring atomic regions collinearity in the directional plane of gradient space. The biggest regions from the atomic region set act as a focus mechanism, governing the merging procedure. Two directional constraints are used for guiding the growing pro-

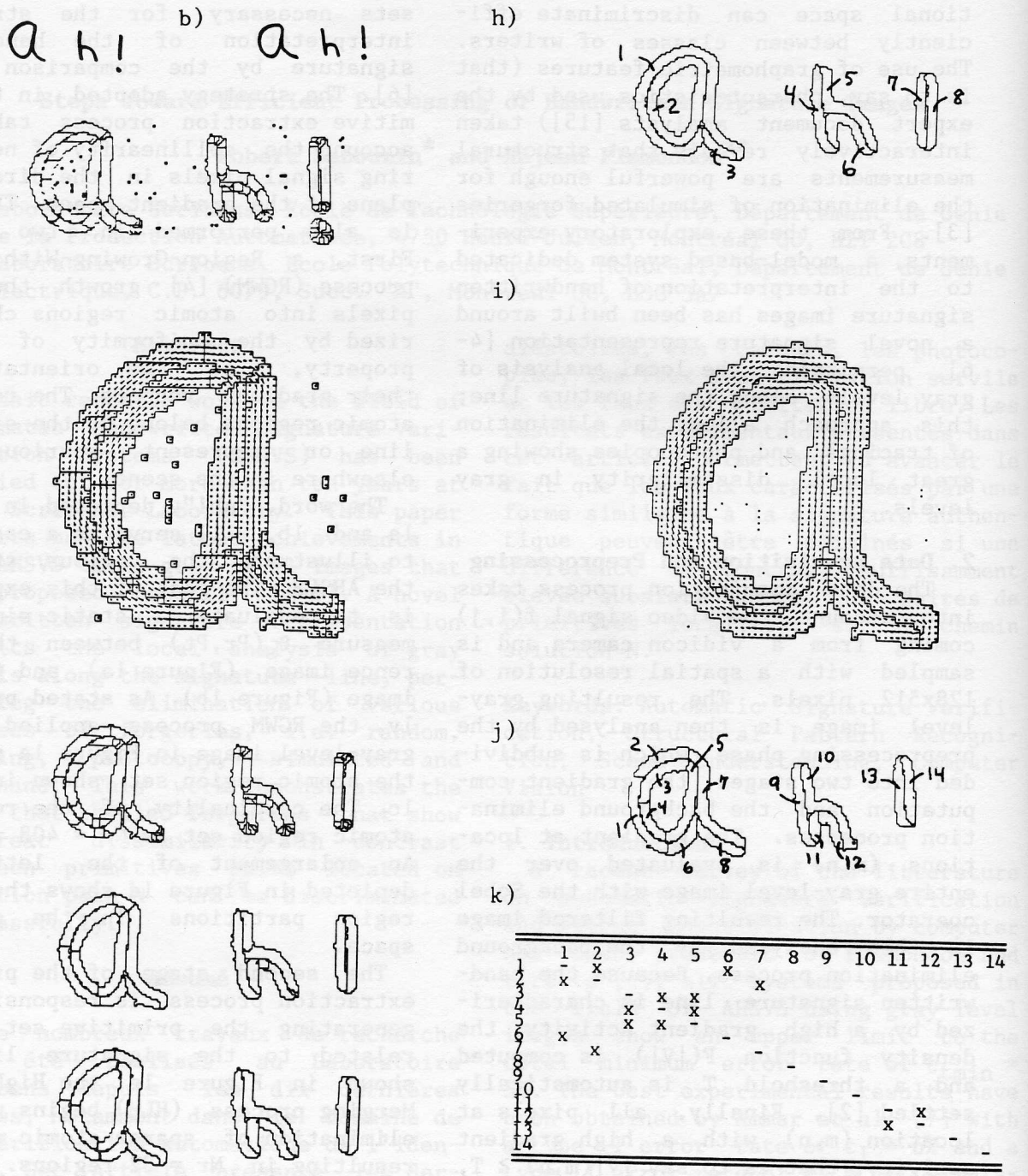


Figure 1: A reference (a) and a test image (b). The atomic region set is shown (c) with the enlargement of the letter "a" in (d). The filtered atomic region set (e) and the resulting reference primitive set Pr produced by the High-Level Merging process (HLM) in (f) to (h). The enlargement of the latter "a" showing the partitions of the reference primitives are depicted in the directional space (i). Finally, the test primitive set Pt (j) and the related adjacency table (k) produced by the HLM process when applied to the test image (b).

cess. A local threshold $\bar{\Theta}_m$ is a requisite for controlling the collinearity of neighbouring pixels along the common border of two atomic regions to be merged. In the present work, the directional threshold is settled to $\bar{\Theta}_m = 45°$. It was shown in [5] that the number of primitives generated by the HLM process tends to stabilize for a value of $\bar{\Theta}_m \geq 45°$. A second constraint is related to the circular variance $\bar{R}_m$ compared to the mixture of the corresponding circular distributions. The circular constraint $\bar{R}_m$ is settled to values corresponding to the circular variance of n angular observations with a uniform distribution on the unit circle, with directional means of 45°, 67.5° and 180° [5]. The resulting primitive set is therefore characterized by a collection of arbitrarily-shaped primitives.

Following this experiment, the primitive sets resulting from the action of the HLM process, varying gradually the circular constraint $\bar{R}_m$ [5], are depicted in Figures 1f to 1h. This hierarchical merging scheme produces primitive sets with cardinalities of Nr = 25, Nr = 19 and Nr = 8 primitives. In Figure 1i, an enlargement of the same letter "a" shows the resulting primitives $Pr_i \in Pr$ related to the representation of a reference handwritten word in the directional space.

The strategy adopted for the comparison of handwritten signature images makes a distinction between the reference primitive set Pr and a test primitive set Pt produced by the primitive extraction process. When a test primitive set Pt is required, the primitive extraction process restricts the final level of merging in the HLM process. The test primitive set Pt shown in Figure 1j reveals a higher level of fragmentation resulting in a test primitive set Pt with a higher cardinality (Nt = 14). This strategy enables the use of a contextual template-matching mechanism in the final merge of test primitives $Pt_v \in Pt$. This partial segmentation scheme allows greater of flexibility in the local interpretation of test primitives $Pt_v \in Pt$, taking into account the intrinsic handwriting variability.

The HLM process is also responsible for the evaluation of adjacency between neighbouring test primitives in the directional space. The adjacency table ADJ is therefore used by the comparison process, i.e. by the Local Interpretation of tests Primitives (LIP) sub-process. Two neighbouring test primitives $Pt_1$ and $Pt_2$ are adjacent if their difference in local directional means, $\bar{\Theta}_1$ and $\bar{\Theta}_2$, computed from gradient vectors located in vicinity of their common border, is less than a directional constraint $\bar{\Theta}_m$ [5]. The resulting adjacency table ADJ computed from the test primitive set Pt depicted in Figure 1j is shown in Figure 1k. This highly restrictive definition of adjacency between pairs of neighbouring test primitives will diminish the computational complexity of the next LIP process.

## 4. Local Interpretation of test Primitives (LIP)

The LIP process is responsible for the labelling of all test primitives $Pt_v \in Pt$, given a reference primitive set Pr. The $A^*$ algorithm previously proposed [8-9] is replaced by a partially informed best first $BF^*$ strategy governed by a new evaluation function $f(n) = f(g(n),h(n))$, where heuristics are embedded in f(n) [6].
The local confidence rating between a test primitive subset $Pt_{v:\gamma} \in Pt$, tentatively labelled as reference primitive $Pr_i \in Pr$, is given by

$$F_i(v) = 1 - f(\gamma) , \qquad (1)$$

where $0 \leq F_i(v) \leq 1$ . (2)

The local confidence rating $F_i(v)$ takes a value near unity for a perfect match in local features between the subset of test primitives $Pt_{v:\gamma} \in Pt$

and the reference primitive $Pr_i \in Pr$. The local interpretation of $Pt_v$ as $Pr_i$ terminates with the set of primitives $TR_i(v) = Pt_{v:\gamma} = \{Pt_v, \ldots, Pt_\gamma\} \in Pt$.

## 5. Global Interpretation of the Scene (GIS)

The first stage of the GIS process involves the evaluation of a static similarity $\vartheta_s(Pr,Pt)$ between the test primitive set Pt and a reference primitive set Pr. Following the example depicted in Figure 1, a state space graph G"=(V",E") is built as shown in Figure 2, from the set of local interpretations $F_i(v) \neq 0$ evaluated at the LIP stage of the analysis.

The state space graph G"=(V",E") is defined as an oriented graph where nodes (states) are grouped in $k \geq 2$ disjoint subsets $V_i$, $1 \leq i \leq k$ (phases). So, the set of nodes V" may be defined as the union of all subsets, as $V" = V_1 \cup V_2 \cup \ldots \cup V_i \cup \ldots V_k$. The static cost (similarity) at node $v \in V_i$ may be defined as

$$S_{i-1,i}(u,v)=(R_{i-1,i}(u,v)+F_i(v))/2 \quad (3)$$

The factor $R_{i-1,i}(u,v)$ represents the similarity in spatial relations (N, S, E, W, N_E, N_W, S_E, S_W and ADJ_TO) between pairs of reference primitives $Pr_{i-1}$ and $Pr_i \in Pr$, and the spatial relations between pairs of related test primitives $Pt_u$ and $Pt_v \in Pt$. Finally, node $v \in V_i$, where the accumulated cost $COST_i(v)$ is maximum, is pushed on list $N_i = v$.

Assuming the use of a Greedy algorithm at the GIS stage, the cost $COST_i(v)$ is therefore defined as [6]

$$COST_i(v) = COST_{i-1}(u) + (\Omega_i * S_{i-1,i}(u,v)), \quad (4)$$

where $u = N_{i-1}$, $v \in V_i$, $\langle u,v \rangle \in E"$, $3 \leq i \leq k-1$

$$\text{and } N_i = v \mid MAX \{ COST_i(v) \}, \quad (5)$$
$$\forall v \in V_i$$

$$0 \leq R_{i-1,i}(u,v) \leq 1, \quad (6)$$
$$0 \leq F_i(v) \leq 1, \quad (7)$$
$$0 \leq \Omega_i \leq 1, \quad (8)$$

Moreover, initial conditions are defined as the relations

$$COST_1(1) = 0, \quad (9)$$
$$N_1 = s, \quad (10)$$
$$COST_2(v) = \Omega_2 * F_2(v) \text{ for } \forall v \in V_2 \quad (11)$$
$$N_2 = v \mid MAX \{ COST_2(v) \}. \quad (12)$$
$$\forall v \in V_2$$

The final step is therefore defined as

$$N_k = t, \quad (13)$$
$$COST_k(t) = COST_{k-1}(u), \quad (14)$$
$$\text{where } u = N_{k-1}. \quad (15)$$

The normalization factor $\Omega_i$ in equation (4) takes into account the ratio, in area, of the reference primitives related to each phase ($Pr_i \equiv V_i$) $\in V"$ to the entire area of the reference primitive set Pr.

$$\Omega_i = AREA(Pr_i) \div AREA(Pr). \quad (16)$$

This permits an additional penalty for primitives not yet included in the definition of V". Finally, $\Omega_i$ emphasizes prominent reference primitives in set V" in the evaluation of a global static similarity measure $\vartheta_s(Pr,Pt)$.

The static similarity $\vartheta_s(Pr,Pt)$ between a reference primitive set Pr and a test primitive set Pt is finally defined as the following relation

$$\vartheta_s(Pr,Pt) = COST_k(t), \quad (17)$$
$$0 \leq \vartheta_s(Pr,Pt) \leq 1. \quad (18)$$

The example depicted in Figure 2 results in a static similarity of $\vartheta_s(Pr,Pt) = 0.8730$ between the two representations Pr and Pt shown in Figures 1h and 1j. The solution path and related cost are presented in Table 1.

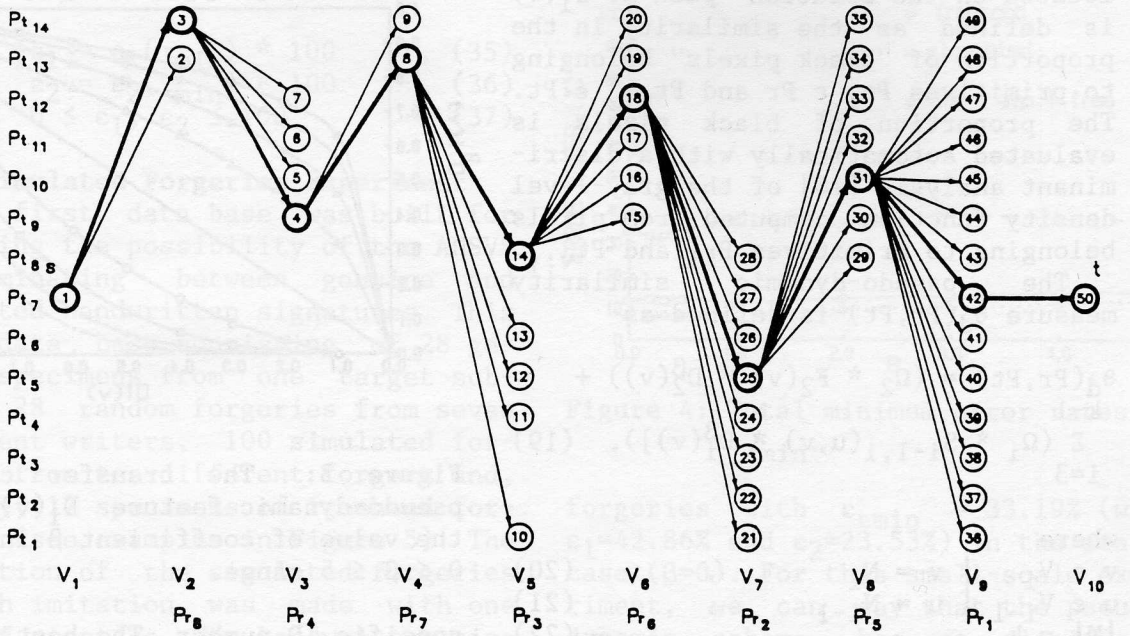


Figure 2: The state space graph G"=(V",E") and the solution path resulting from the comparison of the reference primitive set Pr shown in Figure 1h and the test primitive set Pt in Figure 1j.

Table 1: Solution path from the state space graph G"=(V",E") in Figure 2.

| $V_i$ | Ni | $F_i(v)$ | $R_{i-1,i}(u,v)$ | $COST_i(v)$ | $Pr_i$ | $Pt_{v:\gamma}$ |
|---|---|---|---|---|---|---|
| 1 | 1 | ------ | ------ | 0.00000 | -- | --- |
| 2 | 3 | 0.8404 | ------ | 0.0624 | 8 | { 14 } |
| 3 | 4 | 0.8679 | 0.9116 | 0.1400 | 4 | { 9 } |
| 4 | 8 | 0.8182 | 0.8522 | 0.1974 | 7 | { 13 } |
| 5 | 14 | 0.8093 | 0.9232 | 0.2326 | 3 | { 8 } |
| 6 | 18 | 0.7778 | 0.8680 | 0.2986 | 6 | { 12 , 11 } |
| 7 | 25 | 0.8447 | 0.9234 | 0.4901 | 2 | { 5, 3, 4 } |
| 8 | 31 | 0.9019 | 0.9478 | 0.5933 | 5 | { 10 } |
| 9 | 42 | 0.8275 | 0.9166 | 0.8730 | 1 | { 7, 2, 1, 6 } |
| 10 | 50 | ------ | ------ | 0.8730 | -- | --- |

A pseudo-dynamic similarity measure $\vartheta_d(Pr,Pt)$ is therefore computed at the end of the GIS process with the use of the resulting static solution path N = {s, $\nu_1$, $\nu_2$, ... , $\nu_{k-1}$, t}. By "pseudo-dynamic", we mean the effect of the writing process dynamics, which produces gray levels variation along the signature line. A pseudo-dynamic cost $D_i^{\beta}(v)$ is evaluated from the local analysis of the gray levels inside pairs of primitives $\nu_i = \{Pr_i, Pt_{v:\gamma}\}$

located on the solution path N. $D_i(v)$ is defined as the similarity in the proportion of "black pixels" belonging to primitives $Pr_i \varepsilon Pr$ and $Pt_{v:\gamma} \varepsilon Pt$. The proportion of black pixels is evaluated automatically with a discriminant analysis [16] of the gray-level density function computed from pixels belonging to primitives $Pr_i$ and $Pt_{v:\gamma}$.

The pseudo-dynamic similarity measure $\vartheta_d(Pr,Pt)$ is defined as

$$\vartheta_d(Pr,Pt) = (\Omega_2 * F_2(v) * D_2^{\beta}(v)) + \sum_{i=3}^{k-1} (\Omega_i * S_{i-1,i}(u,v) * D_i^{\beta}(v)]), \quad (19)$$

where

$$v \varepsilon V_i \mid v = N_i \quad , \quad (20)$$

$$u \varepsilon V_{i-1} \mid u = N_{i-1} \quad , \quad (21)$$

$$|N| = k \quad , \quad (22)$$

$$N_1 = s \quad , \quad (23)$$

$$N_k = t \quad , \quad (24)$$

$$0 \leq F_i(v) \leq 1 \quad , \quad (25)$$

$$0 \leq S_{i-1,i}(u,v) \leq 1 \quad , \quad (26)$$

$$0 \leq D_i(v) \leq 1 \quad , \quad (27)$$

$$0 \leq \beta \leq 5 \quad , \quad (28)$$

$$0 \leq \Omega_i \leq 1 \quad . \quad (29)$$

The pseudo-dynamic factor $D_i^{\beta}(v)$ in equation (19) acts as an additional penalty when the cost of the solution path N is revalued. The effect of coefficient $\beta$ on the pseudo-dynamic factor $D_i^{\beta}(v)$ is shown in Figure 3. As term $D_i(v)$ is already normalized in the range of values $0 \leq D_i(v) \leq 1$, the coefficient $\beta$ gives a non-linear transfer function when $\beta \neq 1$. A small difference in terms of the pseudo-dynamic features gives a very high penalty when $\beta$ tends toward $\beta = 5$.

## 6. Experimental Results

Let $\omega_1$ be the class of genuine handwritten signatures and $\omega_2$ be defined as the class of forgeries. A test image from class $\omega_1$ or $\omega_2$ is compared to three reference signature images for a specific writer enrolled in the AHSVS, and identified with a

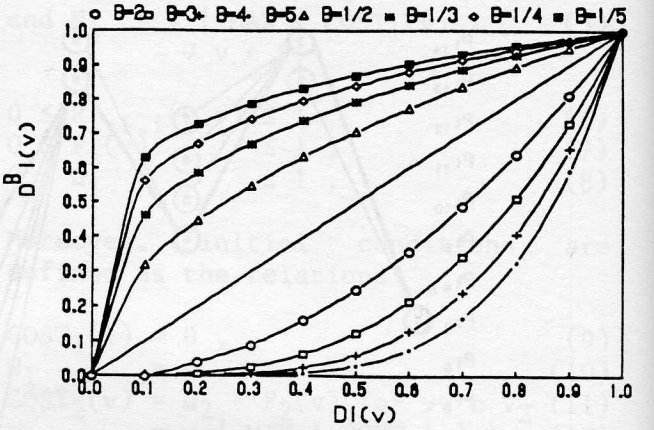


Figure 3: The transfer curves of pseudo-dynamic feature $D_i(v)$, varying the value of coefficient $\beta$ in the $0 \leq \beta \leq 5$ range.

specific ID number. The best similarity $\vartheta_d(Pr,Pt)$ obtained from the comparison process is therefore dispatched to the decision process. All maximum observations $\vartheta_d(Pr,Pt)$ resulting from the comparison of a test image and three reference images for all specimens in class $\omega_1$ and class $\omega_2$ are accumulated in a similarity measure database. The probability functions of resulting maximum similarity measures $\vartheta_d(Pr,Pt)$ are therefore computed considering an equal a priori probability for each class $\omega_1$ and $\omega_2$, say $P[\omega_1] = P[\omega_2] = 0.5$. The experimental results are expressed in terms of total minimum error rates $\varepsilon_{tmin}$ resulting from a scan of the similarity threshold $\tau$ from value zero (0) to one (1) on the similarity scale, so that

$$\varepsilon_t(\tau) = (P[\omega_1] * \varepsilon_1(\tau) + P[\omega_2] * \varepsilon_2(\tau)) * 100 \quad , \quad (30)$$

where $P[\omega_1] = P[\omega_2] = 0.5$ , (31)

and $0 \leq \varepsilon_t(\tau) \leq 100$ , (32)

$0 \leq \tau, \varepsilon_1(\tau), \varepsilon_2(\tau) \leq 1$ , (33)

with $\varepsilon_{tmin} = \text{MIN}_{0 \leq \tau \leq 1} \{ \varepsilon_t(\tau) \}$ . (34)

The Type I ($\varepsilon_1$) and Type II ($\varepsilon_2$) error

rates are expressed as

$$\varepsilon_1 = \varepsilon_1(\tau_{min}) * 100 \quad , (35)$$
$$\varepsilon_2 = \varepsilon_2(\tau_{min}) * 100 \quad , (36)$$
where $0 \leq \varepsilon_1, \varepsilon_2 \leq 100$ . (37)

### 6.1. Simulated Forgeries Experiment

The first data base was built for analysing the possibility of the AHSVS discriminating between genuine and simulated handwritten signatures. This small data base consisting of 28 genuine specimens from one target subject, 28 random forgeries from seven different writers, 100 simulated forgeries from ten different forgers and, finally, 17 specimens of freehand forgeries (see examples in Figure 5). The production of the simulated forgeries through imitation was made with one hour of practice. The handwritten signature model was placed on the table near the sheet used by the forger for imitating the original specimen. No tracing was permitted in this first experiment. In the case of freehand forgeries, the forger has had, over a period of almost five years, many occasions to practice his imitations of genuine specimens, and the imitation was produced from memory.

Many simulation runs were conducted varying the value of parameter $\beta$ (see equation (19)) in the $0 \leq \beta \leq 5$ range. Let us recall that the pseudo-dynamic similarity measure $\vartheta_d(Pr,Pt)$ corresponds to the static case $\vartheta_s(Pr,Pt)$ when factor $\beta=0$. First, all types of forgeries are mixed. The total minimum error rate $\varepsilon_{tmin}$ equals $\varepsilon_{tmin}=11.91\%$ (with $\varepsilon_1=10.71\%$ and $\varepsilon_2=13.10\%$) in the static situation with $\beta=0$. As shown in the Figure 4, the pseudo-dynamic scheme has no effect in this experiment. Numerical results with random, simulated and freehand forgeries taken individually are also presented. All random forgeries are eliminated for this target. Not surprisingly, the elimination of simulated forgeries with $\varepsilon_{tmin} = 7.36\%$ (with $\varepsilon_1=10.71\%$ and $\varepsilon_2=4.0\%$) is better than freehand

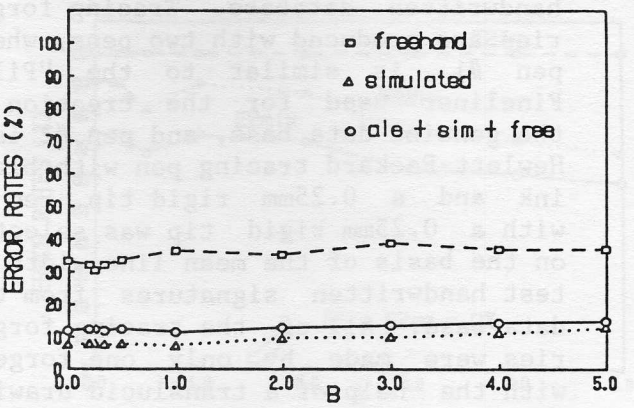


Figure 4: Total minimum error rates $\varepsilon_{tmin}$.

forgeries with $\varepsilon_{tmin} = 33.19\%$ (with $\varepsilon_1=42.86\%$ and $\varepsilon_2=23.53\%$) in the static case ($\beta=0$). For this small-scale experiment, we can say that the pseudo-dynamic scheme has no significant effect on the elimination of skilled forgeries using a "Pilot Fineliner" with a flexible fiber tip.

### 6.2. Random, Tracing and Photocopy Forgeries Experiment

A second experiment with random, photocopy and tracing forgeries was conducted. A data base consisting of 248 genuine handwritten signatures images from eight different writers, divided into 28 test images and 3 reference images per writer has been built. In the random forgery experiment, Class $\omega_1$ is related to the 28 genuine handwritten signatures per writer, while class $\omega_2$ consists of 4 test images from each of the seven other writers. All specimens were written with the same kind of pen, that is to say a "Pilot Fineliner" with black ink and a flexible fiber tip.

The second part of this experiment used the same 248 genuine handwritten signature data base as class $\omega_1$ with 3 genuine references per writer. This time, class $\omega_2$ is related to the tracing forgeries. The following experimental protocol is the same as for the eight writers in the genuine

handwritten database. Tracing forgeries are produced with two pens, where pen #1 is similar to the "Pilot Fineliner" used for the creation of the genuine data base, and pen #2 is a Hewlett-Packard tracing pen with black ink and a 0.25mm rigid tip. Pen #2 with a 0.25mm rigid tip was selected on the basis of the mean line width of test handwritten signatures from the data base. All of the tracing forgeries were made by only one forger, with the help of a translucid drawing table. 10 tracing forgeries were made with each tracing pen, for all target writers. A short example is depicted in Figure 5 where the primitive set of a genuine handwritten signature appears in 5a, with a tracing forgery made using pen #1 and pen #2 are shown in Figures 5e and 5f. A tracing forgery made with pen #1, as depicted in Figure 5e, shows a thicker line width caused by a constant pressure acting on the flexible pen tip during the drawing process. This pictorial effect is a standard characteristic observed in forensic science for this type of forgery made with a flexible fiber pen tip [10,11]. A tracing forgery made with tracing pen #2 using a rigid pen tip is depicted in Figure 5f. The resulting drawing is characterized mostly by a regular line width, and the tremor along the signature line is more visible.

Finally, in the third part of this second experiment, class $\omega_2$ consisted of photocopies of the 224 genuine handwritten signatures in the data base.

Many numerical simulation runs were conducted with the signature data base in an attempt to estimate the performance of the AHSVS with a pseudo-dynamic similarity measure $\vartheta_d(Pr,Pt)$. A global threshold $\tau_{ra} = \tau min$ (equation (34)) was fixed by the random forgeries experiment with eight writers. In fact, random forgeries are generally used as class $\omega_2$ in the evaluation of the global threshold $\tau$

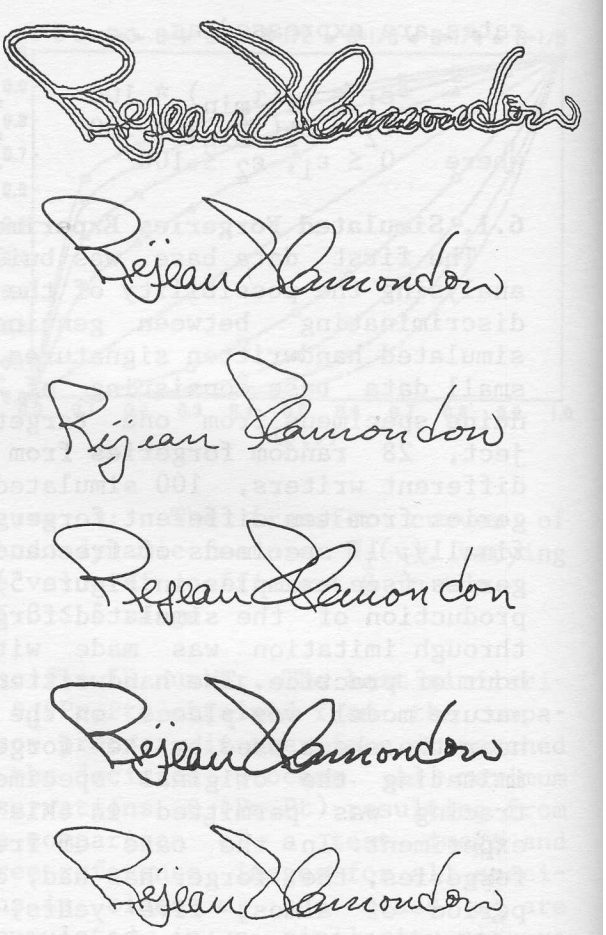


Figure 5: A primitive set (a) related to the genuine handwritten signature depicted in (b). A simulated (c) and a freehand (d) forgeries are followed by a tracing with pen #1 (e) and pen #2 (f).

for the exploitation of commercially AHSVS in real situations [1].

In brief, $\varepsilon_1$ is related to Type I error rates evaluated with the genuine signatures, and $\varepsilon_{2ra}$ to Type II error rates computed with random forgeries. Type II error rates for tracing forgeries, considering all 160 specimens produced with pen #1 and pen #2, are shown as $\varepsilon_{2tr}$, while $\varepsilon_{2trp1}$ and $\varepsilon_{2trp2}$ show the Type II error rates by pen types taken individually. Finally, $\varepsilon_{2ph}$ is related to the Type II error rates for the class of photocopies. The probability function of resulting

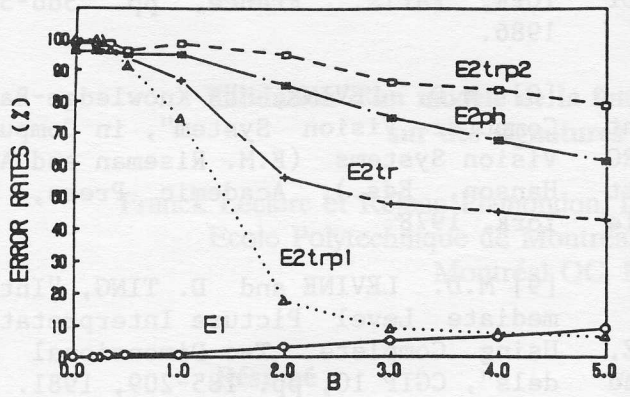


Figure 6: $\varepsilon_1$ and $\varepsilon_2$ error rates evaluated with a common threshold $\tau_{ra}$.

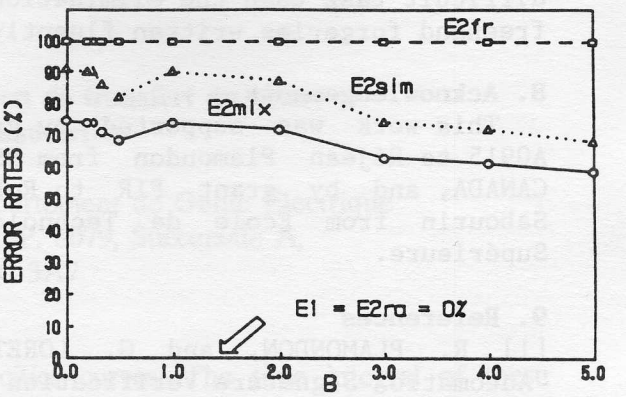


Figure 7: Skilled forgeries experiment evaluated with a common threshold $\tau_{ra}$.

maximum similarity measures $\vartheta_d(Pr,Pt)$ are computed considering equal a priori probability for class $\omega_1$ and each of the $\omega_{2i}$ classes taken individually, that is to say $P[\omega_1] = P[\omega_{2i}] = 0.5$.

In the static case ($\beta$=0), the Type I error rate is $\varepsilon_1$=0.0%, and the Type II error rates related to the $\omega_{2i}$ classes taken individually using a common threshold $\tau_{ra}$ are respectively $\varepsilon_{2ra}$ = 1.34%, $\varepsilon_{2tr}$ = 99.38% and $\varepsilon_{2ph}$=95.98%. Experimental curves depicted in Figure 6 show, in the pseudo-dynamic case ($\beta\neq0$), a clear downward trend in Type II error rates related to tracing forgeries and photocopies, and a corresponding upward trend in Type I error rates. Numerical values obtained with scaling factor $\beta$ settled to $\beta$=5 are $\varepsilon_1$=8.93%, $\varepsilon_{2ra}$=1.79%, $\varepsilon_{2tr}$=42.50% and $\varepsilon_{2ph}$=61.16%. The AHSVS dependency on pen type is clearly visible when tracing forgeries with pen #1 and pen #2 are taken individually. In the best situation ($\beta$=5), their resulting Type II error rates are $\varepsilon_{2trp1}$=6.25% and $\varepsilon_{2trp2}$=78.75%.

### 6.3. Simulated Forgeries with $\tau_{ra}$

Numerical results obtained from the first experiment (section 6.1) with skilled forgeries are plotted in Figure 7, with the same threshold $\tau_{ra}$ evaluated from all random forgeries contained in the AHSVS data base (section 6.2).

The pseudo-dynamic scheme enables a better elimination of simulated forgeries for this related target, considering a Type II error rate of $\varepsilon_{2sim}$=91% in the static case ($\beta$=0) and $\varepsilon_{2sim}$ = 58.62% when $\beta$=5. However, the pseudo-dynamic scheme has no effect on the elimination of freehand forgeries with $\varepsilon_{2fr}$=100% for all $\beta$ values. This fact suggests that the gray levels along the signature line is very similar for genuine and freehand signatures written with this writing tool. Random forgeries were always eliminated for this specific target writer.

## 7. Conclusions

A new scheme is advocated for the design and analysis of automatic handwritten signature verification systems using gray-level images. The use of a novel handwritten signature representation allows the local analysis of contrast evaluated between pairs of primitives located on the static solution path N; this approach permits the elimination of tracings and photocopies having the same shape than genuines signatures, but showing a great local dissimilarity in gray levels along the signature line. As stated by the expert document analysts [10,11], the elimination of tracing forgeries and photocopies seems a less

difficult task than the elimination of freehand forgeries written fluently.

**8. Acknowledgements**

This work was supported by grant A0915 to Réjean Plamondon from NSERC CANADA, and by grant FIR to Robert Sabourin from Ecole de Technologie Supérieure.

**9. References**

[1] R. PLAMONDON, and G. LORETTE, "Automatic Signature Verification and Writer Identification - The State of the Art", Pattern Recognition, Vol. 20, NO. 2, pp. 107-131, 1989.

[2] R. SABOURIN and R. PLAMONDON "Preprocessing of Handwritten Signatures from image Gradient Analysis", Proc. of 8th ICPR, Paris, France, pp. 576-579, 1986.

[3] R. SABOURIN and R. PLAMONDON, "On the implementation of Some Graphometric Techniques for Interactive Signature Verification: A Feasibility Study", Proc. of The Third Int. Symp. on Handwriting and Computer Applications", Montréal, Canada, pp. 160-162, 1987.

[4] R. SABOURIN and R. PLAMONDON, "Segmentation of Handwritten Signature Images Using The Statistics of Directional Data", Proc. of 9th ICPR, Rome, Italy, pp. 282-285, 1988.

[5] R. SABOURIN and R. PLAMONDON, "Segmentation of Handwritten Signature Images: A Structural Approach", submitted to PAMI, 1989.

[6] R. SABOURIN and R. PLAMONDON, "Structural Interpretation of Handwritten Signature Images", submitted to PAMI, 1990.

[7] M. AMMAR, Y. YOSHIDA and T.FUKUMARA, "A New Effective Approach for Off-Line Verification of Signature by Using Pressure Features", Proc. of 8th ICPR, Paris, France, pp. 566-569, 1986.

[8] M.D. LEVINE, "A Knowledge-Based Computer Vision System", in Computer Vision Systems (E.M. Riseman and A.R. Hanson, Eds.), Academic Press, New York, 1978.

[9] M.D. LEVINE and D. TING, "Intermediate Level Picture Interpretation Using Complete Two-Dimensional Models", CGIP 10, pp. 185-209, 1981.

[10] W.R. HARRISON, "Suspects Documents, Their Scientific Examination", Chicago, Nelson-Hall Publishers, 1981.

[11] J. MATHYER, "The Expert Examination of Signatures", Journal of Criminal Law, Criminology and Police Science, Vol. 51, No. 3, pp 122-133, 1961.

[12] F. NOUBOUD, "Contribution à l'étude et à la Mise Au Point d'un Système d'Authentification de Signatures Manuscrites", Thèse de Doctorat, Université de Caen, France, 1988.

[13] F. NOUBOUD, F. CUOZZO, R. COLLOT and M. ACHEMLAL, "Authentification de Signatures Manuscrites par Programmation Dynamique", Congrès PIXIM, Paris, pp 345-360, 1988.

[14] E.R. BROCKLEHURST, "Computer Methods of Signature Verification", NPL Report DITC 41/84, pp. 1-12, 1984.

[15] E. LOCARD, "Traité de Criminalistique", Lyon, Payot, 1936.

[16] N. OTSU, "A Threshold Selection Method from Gray-Level Histograms", IEEE Trans. on Systems, Man, and Cybernetics, Vol. SMC-9, No. 1, pp.62-66, 1979.